J Braz. Soc. Mech. Sci. Eng.
DOI 10.1007/s40430-014-0268-2

TECHNICAL PAPER

Design and analysis of optimal die profile for the extrusion of round SiC DRMM Al 6061 composite billet into hexagonal section

C. Venkatesh · R. Venkatesan

Received: 4 June 2014 / Accepted: 30 October 2014

Abstract Aluminium based matrix composites with silicon carbide as particle reinforcement called discontinuous reinforced metal matrix composites (DRMMs) have excellent mechanical properties like high yield strength, resistance to wear and vibration resistance. But during the development of DRMM composites, compression process like extrusion is an advisable secondary process for homogenous structure. This research work investigates the metal flow behaviour of Al–SiC based DRMM composite through six different die profiles namely third-order polynomial, fourth-order polynomial, cosine, elliptical, hyperbolic and conical geometry. Extrusion load, stress and strain distribution, and metal flow for above said die profiles are predicted using analytical approach upper bound technique and numerical technique finite element method. Cosine and third order polynomial profiles are found to be most optimal in terms of homogenous and less extrusion load requirement. To validate the results, specially made Al–SiC composite through stir casting route was extruded from round to hexagon through an exclusively fabricated cosine die. Results observed from the experiment have good agreement with both analytical and numerical methods.

Keywords Stir casting · Metal matrix composites · Nanoindentation · Upper bound technique · DEFORM-3D · Cosine profile die

List of symbols

L	Length of the die
m	Friction factor
P_{ave}	Average extrusion pressure
r, θ, z	Cylindrical coordinate system
$R(z)$	Die profile
$R'(z)$	First order derivative of $R(z)$
$R''(z)$	Second order derivative of $R(z)$
R_1	Radius at the entry
R_2	Radius at the exit
V_0	Ram velocity
V_r, V_θ, V_z	Velocity components in r, θ and z respectively
ε_{ij}	Strain rate tensor
ζ	Stream function constant
σ_y	Yield stress value of the material
ψ	Stream function

1 Introduction

Advanced material development in the field of engineering applications has made revolutionary changes in the life of engineering components. Metal matrix composites are gaining more significance by replacing the conventional metals and alloys. Aluminium-based metal matrix with silicon carbide as particle reinforcement is technically known as discontinuous reinforcement metal matrix composites (DRMMs). This specific combination of Al–SiC DRMM composites have incredible physical and mechanical properties like higher elastic modulus, yield value, resistance to wear and vibration absorption. These enhanced

Technical Editor: Alexandre Mendes Abrao.

C. Venkatesh (✉)
Department of Mechanical Engineering, Jansons Institute of Technology, Coimbatore 641659, Tamilnadu, India
e-mail: venkyachvsh@yahoo.co.in

R. Venkatesan
Department of Mechanical Engineering, Sona College of Technology, Salem 641659, Tamilnadu, India

Published online: 13 November 2014

superior properties of this composite find more useful in construction of aerospace, satellite vehicles, automobile and advanced sports equipments.

As a primary processing technique to develop the metal matrix composite, either stir casting route or powder metallurgy technique has been followed. But these processing techniques often develop the composites with defects like porosity, non uniform grain structure and inhomogeneous reinforcement distribution. Another defect is weak bonding between matrix and reinforced material owing to their difference in density. These defects are rectified or relieved, when the composites are fed into extrusion because, during the extrusion, the materials not only deform into required shape but also it attains a refinement in its microstructure to a greater extent. Hence the extrusion of the metal matrix composites with particle reinforcement is an inevitable secondary process for their microstructure development.

A number of research works have been carried out on streamlined extrusion. Narayanasamy et al. [1] have suggested the streamlined extrusion die by taking the die profile as cosine function and have analysed through upper bound technique and compared the results with concave and straight-tapered die, but they have considered the material as aluminium. Naraynasamy et al. [2] did the same analysis for streamlined die by considering the die profile as Bezier curve. Venkatareddy et al. [3] have attempted to find an optimal die profile for axisymmetric extrusion through a pure analytical approach of a combined upper bound and slab method. They have compared the results of eight different die profile shapes and they have concluded that the cosine and fourth order polynomials are the best amongst the profiles considered. Seo et al. [4] have conducted a research work regarding the influence of die profile over the mechanical properties of silicon carbide reinforced aluminium composite fabricated by melt stirring. They have concluded that the tensile strength of extruded billet has been increased by 20–30 % and also homogeneous distribution of reinforcement has been improved.

Influence of particle reinforcement of Al_2O_3 with aluminium as matrix material has been studied by Herba et al. [5] using DEFORM package, finally they have validated that the higher load-stroke curve were recorded for higher content of Al_2O_3 particle. Effect of dead metal zone and frictional contact between the die and Sic reinforced Al 6063 composite have been investigated by Nair et al. [6]. These researchers have stressed and predicted that there are two sections of dead metal zone developed during deformation of Al–Sic composite out of which one zone allowed the material to flow in smaller gradient and another allowed none of the material to flow. Classically, finite element approach has been initiated by the authors Gordan et al. [7] and several simulations were made using numerical tool DEFORM 3D to predict the extrusion die shape which produces minimum distortion in axisymmetric product. Forward extrusion of square geometry from a round section through a straight tapering die was analysed using both updated Lagrangian and the coupled Eulerian–Lagrangian finite element meshing technique by Gouvia et al. [8]. They have come up with the results, that the coupled Eulerian–Lagrangian mesh techniques are more efficient. Design of streamlined extrusion die to extrude an aluminium round billet into hexagonal section has been carried out by this same author Venkatesh et al. [9] using UBT and FEM, and they compared the results with the experimental results to validate the cosine profile is a best streamlined profile.

Most of the previous research work focused to register the benefit of streamlined profile through various techniques by considering the billet as aluminium or any other metals, but very few attempts have been made towards the extrusion of DRMM composite, but it is mandatory for the present environment to insight over the extrusion of composites due to their increasing application in different industries. In this study, keen attention was paid to bring out an exact and efficient die profile with proper specifications to extrude an advanced material like silicon carbide reinforced metal matrix composite. Moreover, this study has diverted into an industrially benefited hexagonal section. To investigate the optimal profile, there are six different die profile geometry like fourth-order polynomial, third-order polynomial, cosine, elliptical, hyperbolic and conical were utilised.

2 Geometry of die profile

In extrusion, mechanical properties of the billet material, extrusion ratio, frictional condition between die-workpiece interface, and the die profile are the predominant parameter that directly influences the product quality [10]. Study of frictional condition and effect of die profile to impart a homogeneous deformation of material flow becomes very complex in analytical way. Reduction of dead metal zone and frictional effect between die—workpiece interfaces ensures the homogeneous metal flow; this has been proved

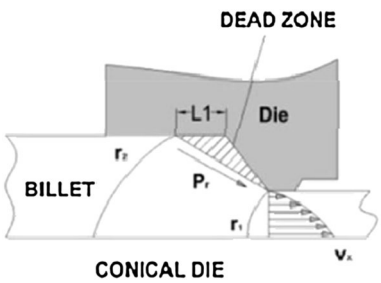

Fig. 1 Extrusion through conical die

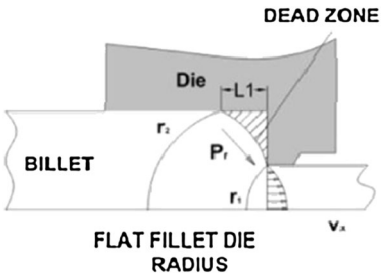

Fig. 2 Extrusion through fillet radius die

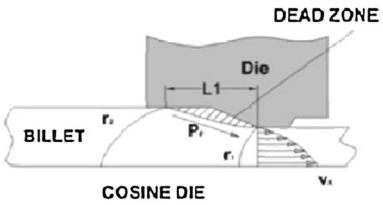

Fig. 3 Extrusion through cosine die

by many researchers by redesigning the die profile. But most of the research articles dealt with conventional conical die with different cone angle [10]. The effect of dead metal zone during extrusion is schematically represented in Figs. 1, 2 and 3.

3 Material and method

3.1 Development of composite billet

The Al–SiC DRMM composite was manufactured through stir casting route. AA 6061 aluminium alloy was used as a matrix material, its chemical composition has been presented in Table 1. SiC granules with particle size of 45 µm according to availability and volume fraction 15 % was used as a reinforced material as shown in Fig. 4. Percentage of volume fraction would influence the hardness and strength [4]. The chemical composition of SiC particles has also been presented in Table 2.

Initially, the stir casting process was started by melting AA6061 matrix material into 750 °C in a graphite crucible coated with wolfra coat, within the resistance-heated furnace. Next, SiC particle preheated up to 450 °C were mixed into the molten bath of AA6061. The complete molten bath with reinforced material and matrix material were stirred by a stirrer at 700 rpm for 30 min. The argon gas was made to flow through the mixing and stirring phase at a rate of 15 gm/min. As soon as the stirring process has over, the material mixture was poured into a specially made mould of 25 mm in diameter and 60 mm length. The material was allowed to cool in open atmosphere, and then the material was machined to a 10-mm diameter and 25 mm in length of cylindrical section.

3.2 Microscopic examination

The part of the casted composite material was finished to the 1 cm cube. The specimen material was fully ground to maximum surface finish and then cleaned by acetone. To determine the value of young's modulus and the hardness of the material, the nano-indentation set up were employed. The prepared specimen was fixed on a metal base firmly with special adhesive under the Berkovich-type indenter. More than 40 indentations were made over the surface of the specimen at various places with the load ranging from 11 to 67 mN. The depth of penetration beneath the specimen surface was observed and recorded for every indentation from the nano-indenter in nanoscale as shown in Fig. 5. From the extracted results, the load displacement curve has been plotted as shown in Fig. 6.

The known geometry of the indenter then allows the size of the area of indentation to be determined. Elastic modulus and hardness of the specially developed composites were calculated from the results of nano-indenter [11], which in turn leads to allow the magnitude of the yield strength to be determined.

Table 1 Chemical compositions of an Al alloy (wt%)

Al	Si	Fe	Cu	Mn	Mg	Cr	Zn	Ti
Bal	0.65	0.23	0.22	0.03	0.84	0.22	0.1	0.01

Table 2 Chemical compositions of silicon carbide particle

SiC	Si	SiO_2	C	Fe	Al	CaO	MgO
98.65	0.15	0.63	0.36	0.08	0.08	0.05	0.03

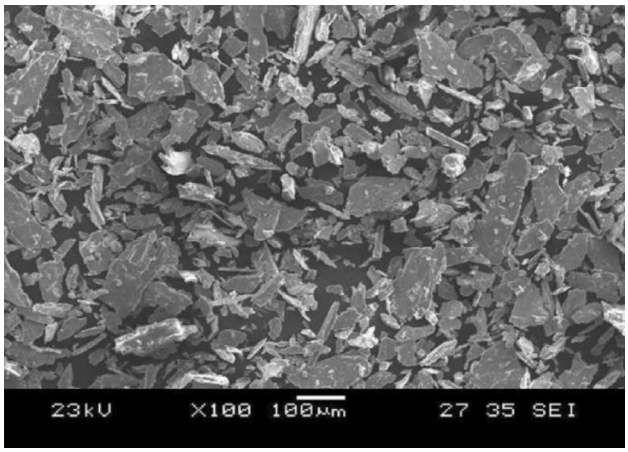

Fig. 4 SEM image of SiC particles

4 Upper bound analysis

4.1 Derivation of velocity and strain rate fields

During an execution of upper bound technique to analyse plastic deformation, an efficiently formulated velocity field is required to ensure the accuracy of the final solution. The velocity components must satisfy the incompressibility condition in order to be kinematically admissible.

The billet material is assumed to be rigid at the outside, the entry and the exit of the die section, hence the velocity profiles at these sections are assumed to be uniform. An assumption is extended that the flow pattern of the material in the deformation zone can be represented in the same functional form as the die profile. In the present work, the geometric shape of the die profile is considered to be a key variant for optimal effect. Hence, six different die profile geometries have been considered.

4.1.1 Third-order polynomial die profile

This die profile is shown in Fig. 7 and is represented by the function

$$R(Z) = R_1 + (R_1 - R_2)\left[2\frac{Z^3}{L^3} - 3\frac{Z^2}{L^2}\right]. \tag{1}$$

4.1.2 Fourth-order polynomial die profile

This die profile is shown in Fig. 8 and is represented by the function

$$R(Z) = R_1 + \frac{6cLk(2-3cL)}{L^2}Z^2 + \frac{4k\left(3(cL)^2-1\right)}{L^3}Z^3 + \frac{3k(1-2cL)}{L^4}Z^4. \tag{2}$$

4.1.3 Cosine die profile

This die profile is shown in Fig. 9 and is represented by the function

$$R(Z) = \frac{R_1 + R_2}{2} + \frac{R_1 - R_2}{2}\cos\frac{\pi Z}{L}. \tag{3}$$

4.1.4 Elliptical die profile

This die profile is shown in Fig. 10 and is represented by the function

$$R(Z) = \sqrt{R_1^2 - (R_1^2 - R_2^2)\left(\frac{Z}{L}\right)^2}. \tag{4}$$

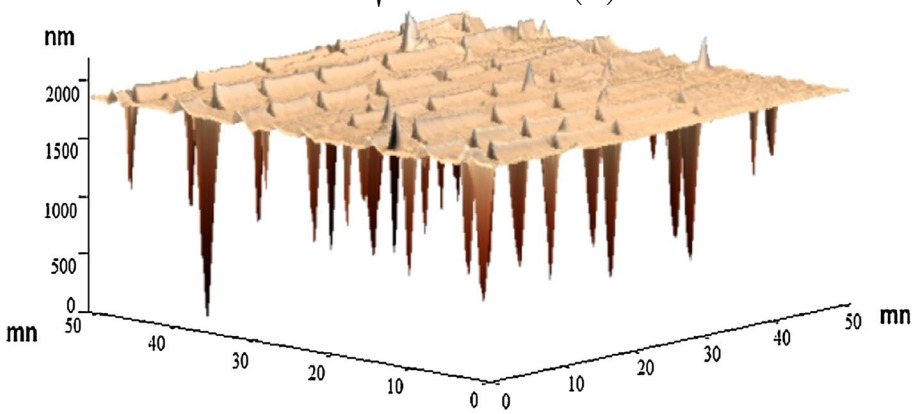

Fig. 5 Morphology of nano-indenter

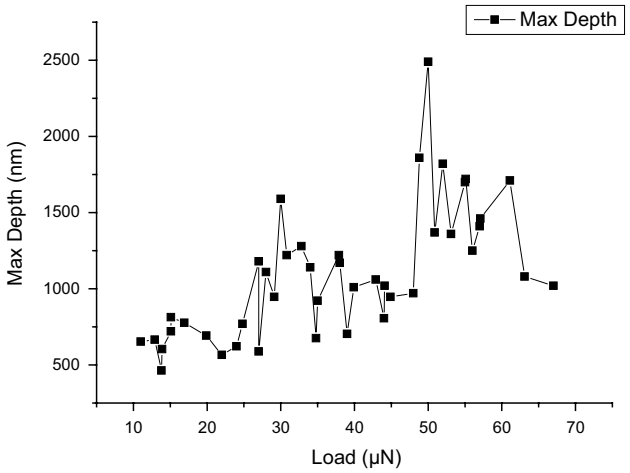

Fig. 6 Load-displacement curve

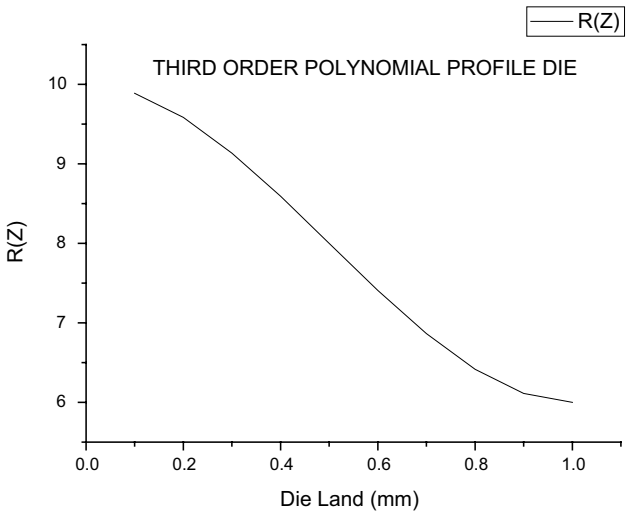

Fig. 7 Third-order polynomial profile

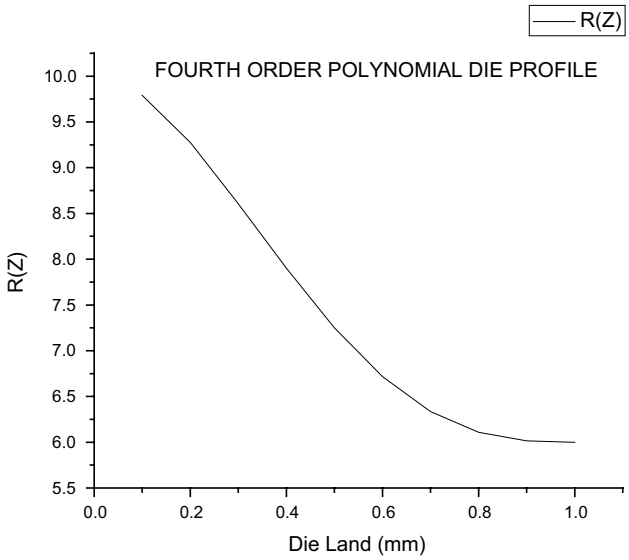

Fig. 8 Fourth-order polynomial profile

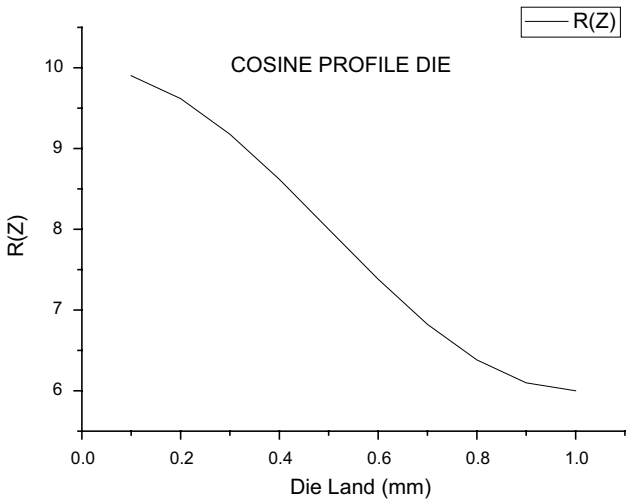

Fig. 9 Cosine profile

4.1.5 Hyperbolic die profile

This die profile is shown in Fig. 11 and is represented by the function

$$R(Z) = \sqrt{R_2^2 + (R_2^2 - R_1^2)\left[1 - \left(\frac{Z}{L}\right)^2\right]}. \tag{5}$$

4.1.6 Conical die profile

This die profile is shown in Fig. 12 and is represented by the function

$$R(Z) = R_1 + \frac{R_1 - R_2}{2} Z. \tag{6}$$

In order to satisfy the condition of uniformity of axial velocity (V_0) at the entry section, the stream function can be assumed as

$$\psi = \frac{V_0 R_1^2 \xi^2}{2}. \tag{7}$$

The velocity components V_r, V_θ and V_z are analytically derived in terms of the die profile from the derivatives of the stream function for the six different profile function as

$$V_Z = \frac{1}{r}\frac{\partial \psi}{\partial r} = \frac{V_0 R_1^2}{R^2(Z)} \tag{8}$$

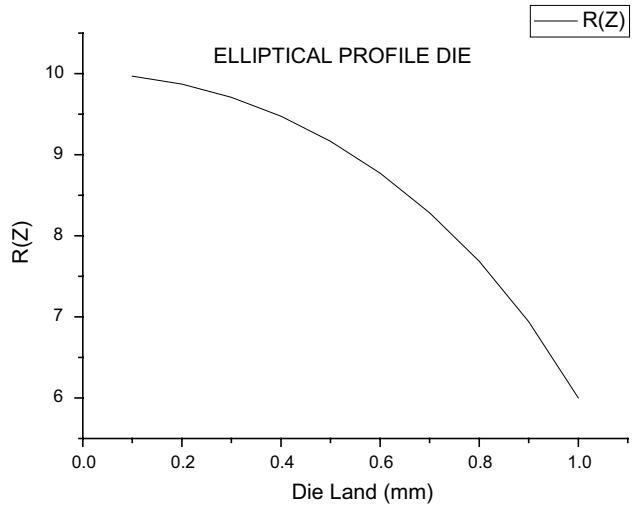

Fig. 10 Elliptical profile

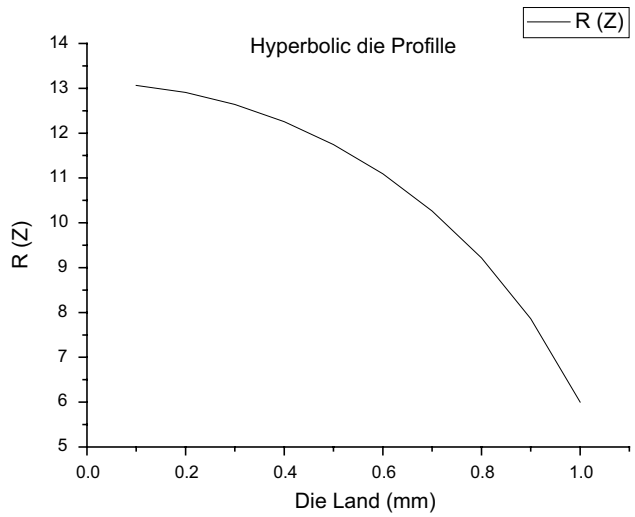

Fig. 11 Hyperbolic profile

$$V_r = -\frac{1}{r}\frac{\partial \psi}{\partial z} = \frac{\xi V_0 R_1^2 R^1(Z)}{R^2(Z)} \tag{9}$$

$$V_\theta = \frac{V_r}{r} = \frac{\xi^2 V_0 R_1^2 R^1(Z)}{R(Z)}. \tag{10}$$

From the velocity field Eqs. (7), (8), (9) and (10) the strain rate components can be derived as

$$\varepsilon_{rr} = \frac{\partial V_r}{\partial r} = \frac{V_0 R_1^2 R^1(Z)}{R^3(Z)} \tag{11}$$

$$\varepsilon_{zz} = \frac{\partial V_Z}{\partial z} = -2\frac{V_0 R_1^2 R^1(Z)}{R^3(Z)} \tag{12}$$

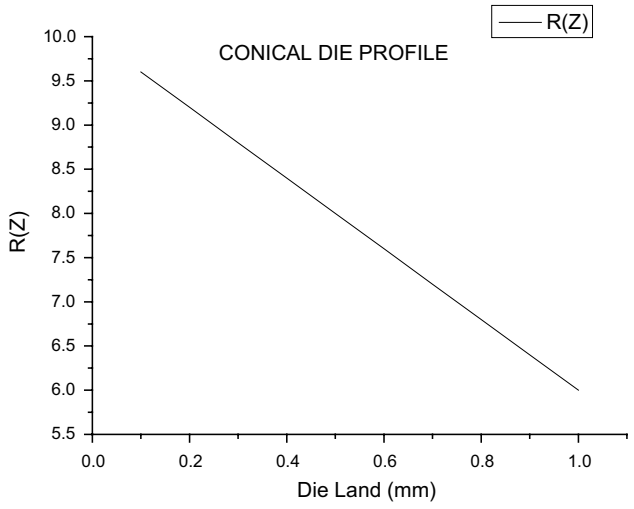

Fig. 12 Conical profile

Table 3 Extrusion and frictional load through UBT

S. no.	Name of the profile	Extrusion load (KN)	Frictional load (KN)
1	Third order	147.67	2.067
2	Fourth order	371.56	10.22
3	Cosine	141.34	1.55
4	Elliptical	981.44	24.14
5	Hyperbolic	2,156.7	19.18
6	Conical	320	13.24

$$\varepsilon_{\theta\theta} = \frac{1}{r}\left[\frac{\partial V_\theta}{\partial \theta} + V_r\right] = 2\frac{V_0 R_1^2 R^1(Z)}{R^3(Z)} \tag{13}$$

$$\begin{aligned}\varepsilon_{r\theta} &= \frac{1}{2}\frac{\partial V_\theta}{\partial r} - \frac{V_\theta}{r} + \frac{1}{r}\frac{\partial V_r}{\partial \theta} \\ &= -\frac{V_0 R_1^2 R^1(Z)}{2R^2(Z)}\frac{1}{R(Z)} - 3\xi\end{aligned} \tag{14}$$

$$\varepsilon_{\theta z} = \frac{1}{2}\frac{\partial V_\theta}{\partial Z} + \frac{1}{r}\frac{\partial V_Z}{\partial \theta} = -\frac{3V_0 R_1^2 R^{II}(Z)}{2R^4(Z)} \tag{15}$$

$$\varepsilon_{rz} = \frac{1}{2}\frac{\partial V_r}{\partial r} + \frac{\partial V_z}{\partial r} = \frac{-V_0 R_1^2 R^I(Z)}{R^3(Z)}\left[1 + \frac{1}{\xi}\right], \tag{16}$$

where $R^I(Z) = \frac{dR(z)}{dz}$ and $R^{II}(Z) = \frac{d^2R(z)}{dz^2}$

4.2 Upper bound Theorem

The total power consumption (J) required to deform the circular billet into hexagonal section through the six different

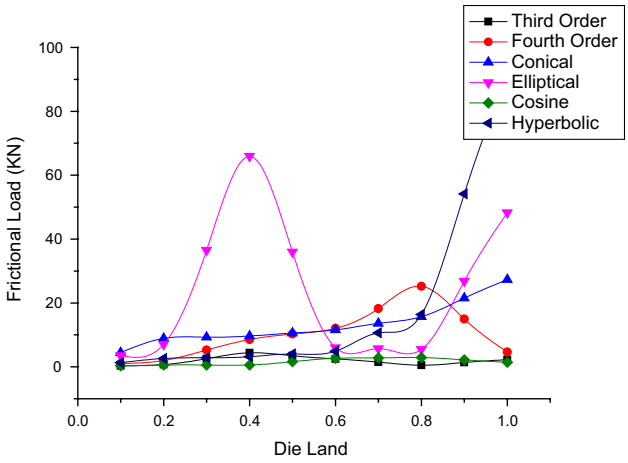

Fig. 13 Frictional load graph for various profiles

die profile is denoted as the sum of the power losses due to the plastic deformation inside the die (W_i), due to the velocity discontinuities at the entry (W_e) and at the exit (W_f) and due to the frictional resistance at the interface between die and material (W_s)

$$J = W_i + W_e + W_f + W_s. \tag{17}$$

But as far as streamlined die profile is concerned, that the velocity components at the entry and exit are uniform, then the equation becomes as

$$J = W_I + W_s \tag{18}$$

Power loss due to internal deformation:

$$W_I = \frac{2\sigma_y}{\sqrt{3}} \iint_v \sqrt{\frac{\varepsilon_{ij}\varepsilon_{ij}}{2}} \mathrm{d}v \tag{19}$$

$$W_I = \frac{2\sigma_y}{\sqrt{3}} \int_0^z \int_0^r \int_0^\theta \sqrt{\frac{\left(\varepsilon_{rr}^2 + \varepsilon_{\theta\theta}^2 + \varepsilon_{zz}^2\right) + \left(\varepsilon_{r\theta}^2 + \varepsilon_{\theta z}^2 + \varepsilon_{rz}^2\right)}{2}} \mathrm{d}\theta \mathrm{d}r \mathrm{d}z. \tag{20}$$

Power loss due to frictional resistance:

$$W_s = \frac{m\sigma_y}{\sqrt{3}} \int_0^z \int_0^\theta \sqrt{V_r^2 + V_\theta^2 + V_z^2} \sec\alpha \left| \frac{\partial(r,z)}{\partial(\theta,z)} \right| \mathrm{d}\theta \mathrm{d}z. \tag{21}$$

The angle α is the angle of inclination of the element of the die surface for all six die profiles with respect to the projected surface of the element on the rz plane.

Knowing the velocity components, strain rate components of the individual die profile of the six different profiles, the volume integral was carried out using Simpson's one-third techniques. The yield value of the material has substituted from the microscopic results of the nano-indenter apparatus. The average extrusion load (P_{ave}) and relative stress (R_s) can be determined from the total power consumption as follows,

$$\mathrm{P_{ave}} = \frac{W_i}{\pi R_{1V_0}^2}. \tag{22}$$

The results computed by solving the Eqs. (20), (21) and (22) are tabulated in Table 3.

5 Finite element analysis

Significance of optimal die profile is insisted by drawing a comparison between six different geometry of profile like Fourth-order polynomial, third-order polynomial, cosine, elliptical, hyperbolic and conventional conical through finite element method. To analyse the die profiles in FEM, DEFORM 3D V6.1 [12] software was utilised. The die geometry containing hexagonal and cylindrical portions were created as solid model using ProE. The inter-junction between the cylindrical and hexagonal portion was extended as die land measuring a length of 1. The profile of die land was made by the above said six different curves. All the six solid model of die profiles were exported to DEFORM 3D V 6.1 as STEP file.

A SiC–Al composite billet measuring 25 mm long and 10 mm diameter was meshed into 36,767 tetrahedral elements where the aspect ratio was kept as unity. Mechanical properties of the already prepared composite have been derived using nano-indenter setup and were loaded as material properties in DEFORM database. A friction factor of 0.3 and ram velocity as 1 was assumed for all six types of profiles. The entire simulation was designed to complete in 100 steps.

After the completion of simulation, each and every data was extracted from the FEM analysis to evaluate each distortion criterion. Data extracted along the distorted grid line allows the minimum average axial displacement, average shear strain, and average effective strain. To extract the data efficiently, the point tracking options in the DEFORM-3D post processor was found very useful.

6 Results and discussion

It is well understood from the literature of extrusion [10] deformation that the rate of deformation from the entrance of the die to the exit point is diminishing. Similarly, the force required to extrude the billet also decreases from the peak point at the entrance of the die to zero at the die exit. Strain rate and shear deformation are utmost peak point at the entrance of the die, hence the die entrance zone is the highest deformation zone. Inhomogeneous strain gradient

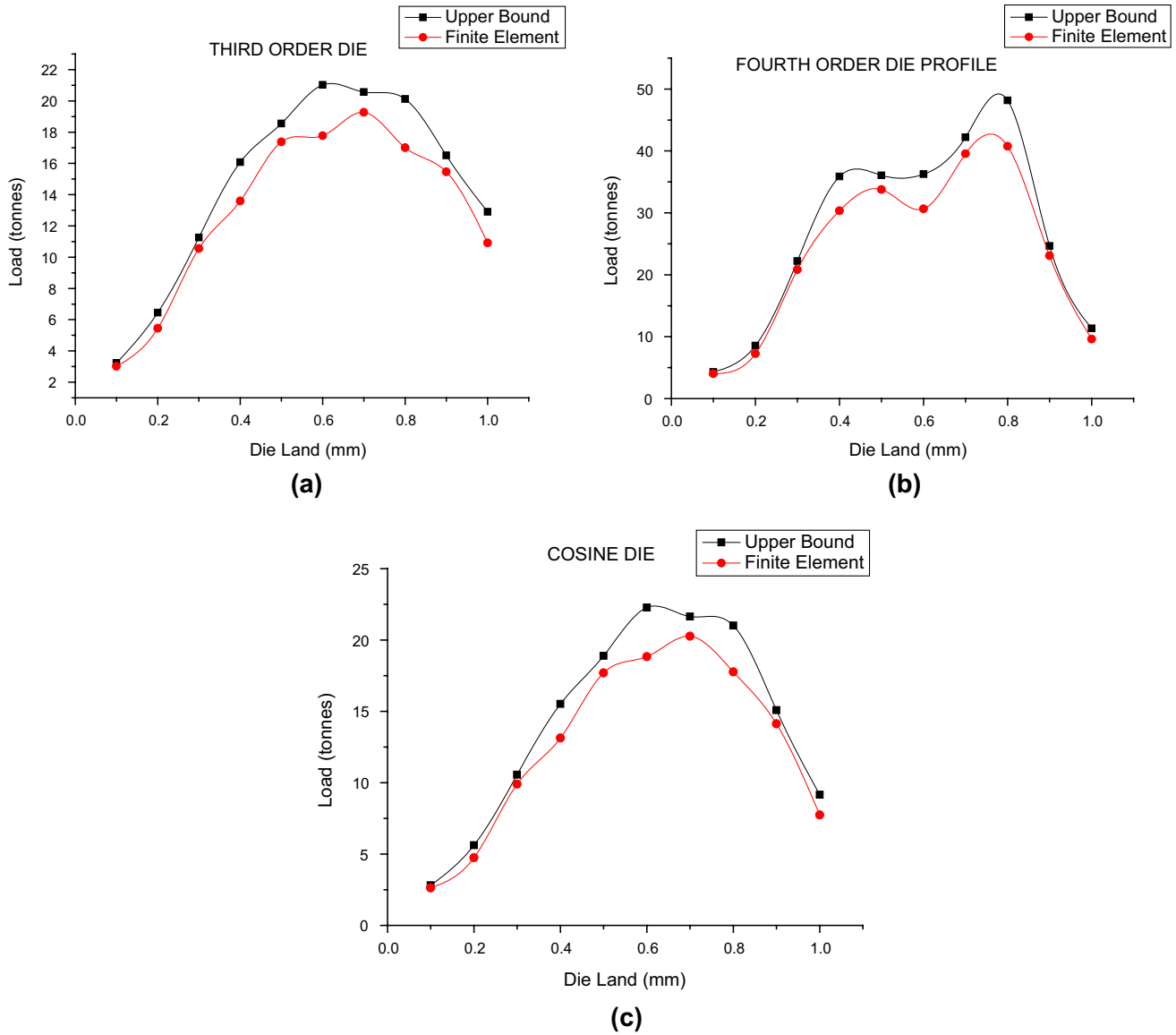

Fig. 14 Extrusion load curves b fourth order, **b** third order, **c** cosine

at the outer and central part of the billet causes the dead metal zone near the die entrance.

But during the SiC DRMM composite extrusion, the SiC particles are compelled to move along the matrix material. Majority of the particles align with the flow of matrix material, but some of them move with abrading action at the die-billet interface [6]. Abrading behaviour of these particles causes the scratching effect on the die land surface.

Also few of the SiC particles forced to deform imposes a challenge by developing a huge friction between the die-billet interfaces. It is observed from the previous study that the die surface is found to be scratched due to the flow of SiC particles and matrix materials, further some of the SiC particles propagate the scratches into micro grooves. Some of the SiC particles are embedded into the wear mark or groove scratched by the previous particles either in die entrance or in die bearing surface. If the embedded particles retain their location, some matrix material and few SiC particles may be accumulated behind these embedded particles and act as a part of the die profile, thereby increasing the extrusion load and affecting the surface properties of the extrudate.

It is keenly observed from the Figs. 7 and 9 third-order polynomial and cosine profiled die geometry has got a initial curvature effect at the die entrance which facilitates the free flow of both matrix and reinforced SiC particles without causing any adhering and scratch. But in the Figs. 10, 11 and 12 enlightens the fact that the absences of initial

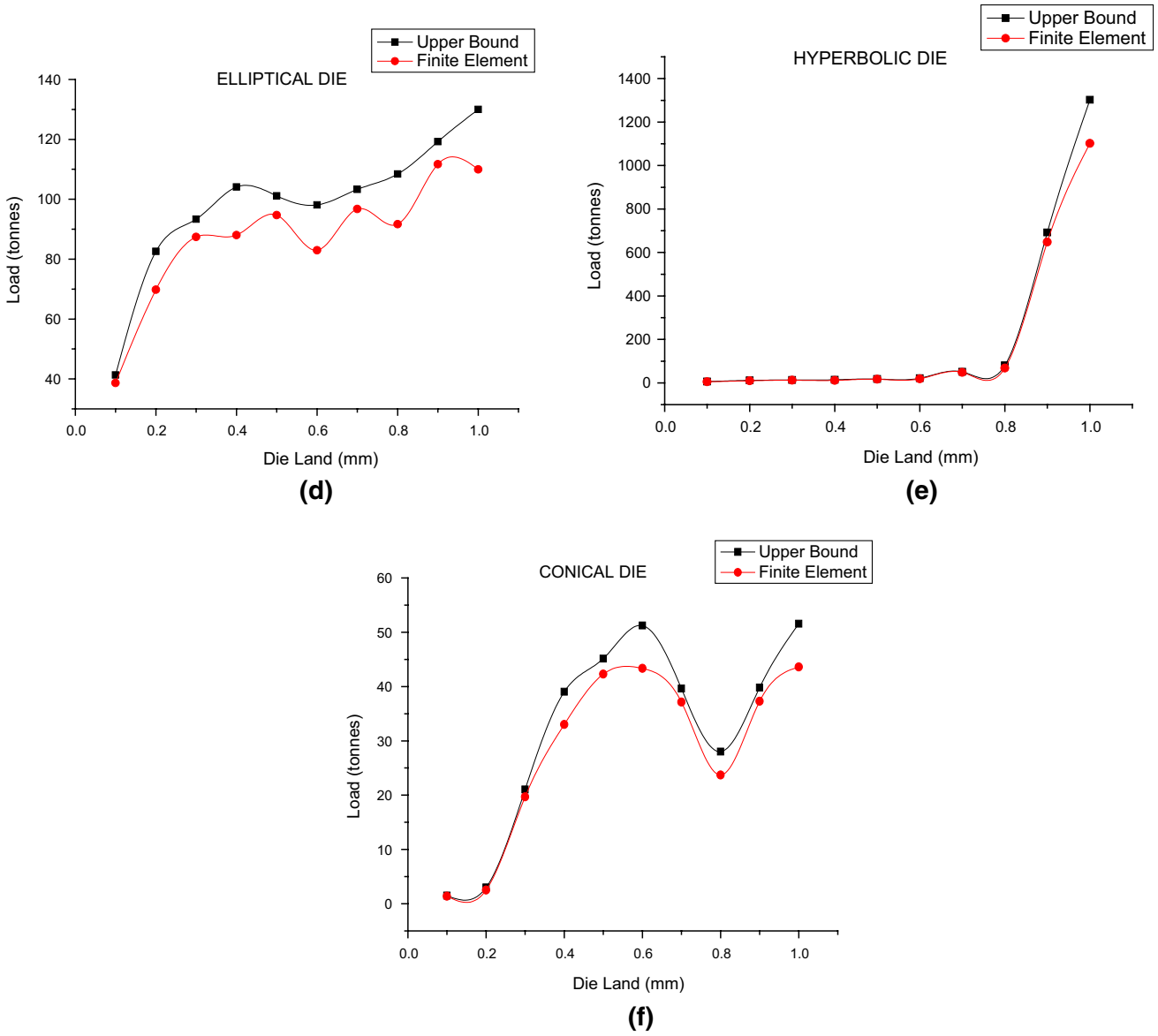

Fig. 15 Extrusion load curves **a** elliptical, **b** hyperbolic, **c** conical

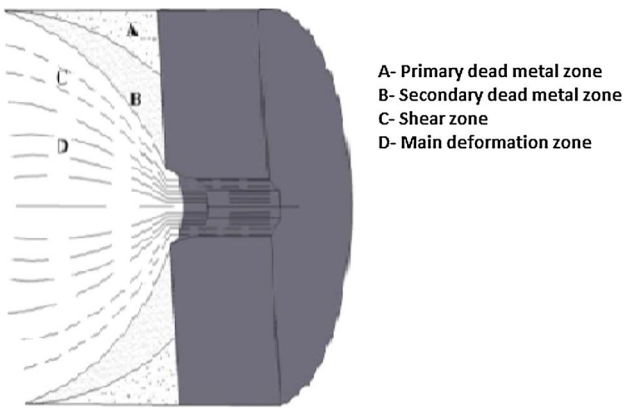

Fig. 16 Development of dead metal zone

curvature effect on conical, elliptical, hyperbolic die profiles causes the flow of matrix and the SiC particles with adhering behaviour and scratch effect on the die entrance and the bearing surfaces. This damage mechanism prevails on these profiles reserves the negative factor such as higher extrusion load requirement, development of friction and non homogeneous material flow and strain development. The comparative graph plotted for the frictional load calculated using upper bound technique shown in Fig. 13 depicts the frictional load requirement for the six different profiles. Cosine profiled die is declared to be a optimal die by encountering a very lesser average frictional load of 1.62 kN than the highest average frictional load of 26.55 kN of elliptical die.

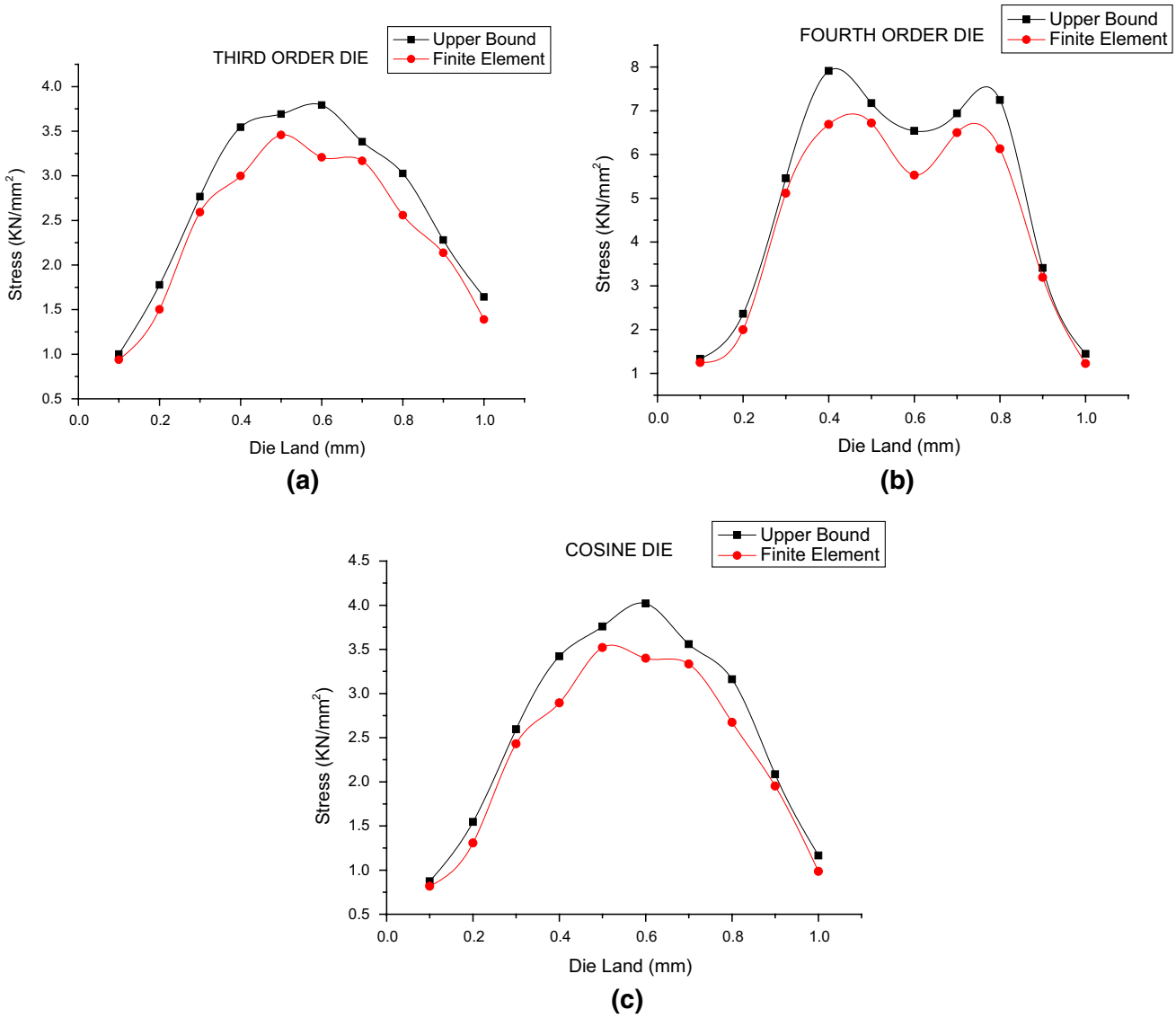

Fig. 17 Stress distribution **a** third order, **b** fourth order, **c** Cosine

The different load curves arrived from UB and FEM methods for six different profiles shown in Figs. 14 and 15 assure the fact that the cosine profile requires lesser load than the rest of the five different profiles. Development of friction, inhomogeneous material flow and inhomogeneous strain gradient are in lesser effect for the cosine die, that is why it is firmly learnt that the cosine die is the best among the rest of the dies by consuming a lesser extrusion load of 14.5 tonnes both in UBT and FEM methods.

It is also comprehended from the research literature, during extrusion of composite material, development of dead metal zone near the die entrance has got two different sections as shown in Fig. 16. Area A shows the actual dead metal zone which does not allow any material to flow, the compressed inactive material acts as funnel to direct the material towards the die entrance. Area B is called as secondary dead metal zone comes after A which allows very minimal material to flow to the die bearing [6]. The SiC particles in this zone participates in agglomeration of their own group which in turn acts as barrier for uniform flow and also increases frictional effect from the die entrance to die land.

From the simulation results shown in Fig. 19. The material flow and strain gradient are homogeneous for cosine and third-order die profile because effect of agglomeration of the SiC particles near the die entrance is very minimal than the rest of the die profiles. The nature of profile with initial curvature of cosine and third-order die ensures the homogeneity in plastic deformation and material flow by averting the probability of agglomeration of SiC particles near the

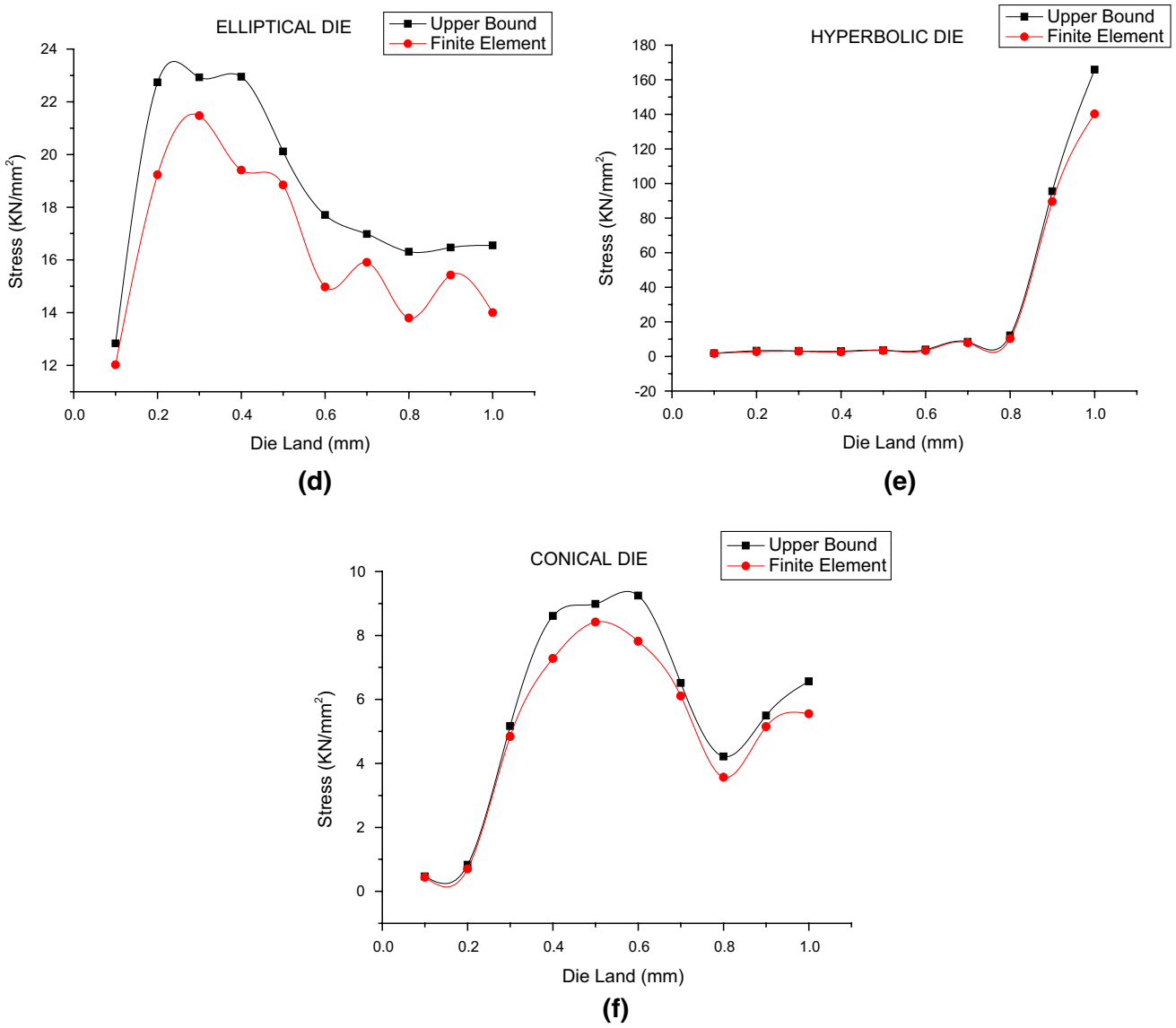

Fig. 18 Stress distribution **a** elliptical, **e** hyperbolic, **f** conical

die entrance. From the Figs. 17 and 18 which emphasizes the stress development for each die profile throughout the entire die length computed through upper bound and finite element method. During the plastic deformation, the development of stress is in lower magnitude when it is extruded through cosine and third-order polynomial profile where as stress development is in higher magnitude when it is flowing over the rest of four die profiles. Higher dead metal zone accompanying with greater frictional force causes the deformation of the outer zone much higher than the central zone which in turn develops the higher stress values.

This inhomogeneous deformation phenomenon stimulates the higher load requirement to deform the central zone further. The effect of uniform curvature of cosine and third-order polynomial die profiles ensures the lesser extrusion load requirement, lesser frictional effect, and homogeneous strain gradient and homogeneous material flow.

7 Experimental study

To carry out an experimental study, the hexagonal extrusion die with cosine profile as die land geometry is made out of chrome-vanadium tool steel through CAD/CAM using wire cut EDM machine as shown in Fig. 20. The billet made out from SiC DRMM Al-6061 composite, casted through stir casting route was machined for 9 mm diameter and 25 mm length was fed into 45 Tonne capacity cranked type SEYI make press to extrude the required hexagonal shape. The extruded product is shown in Fig. 21.

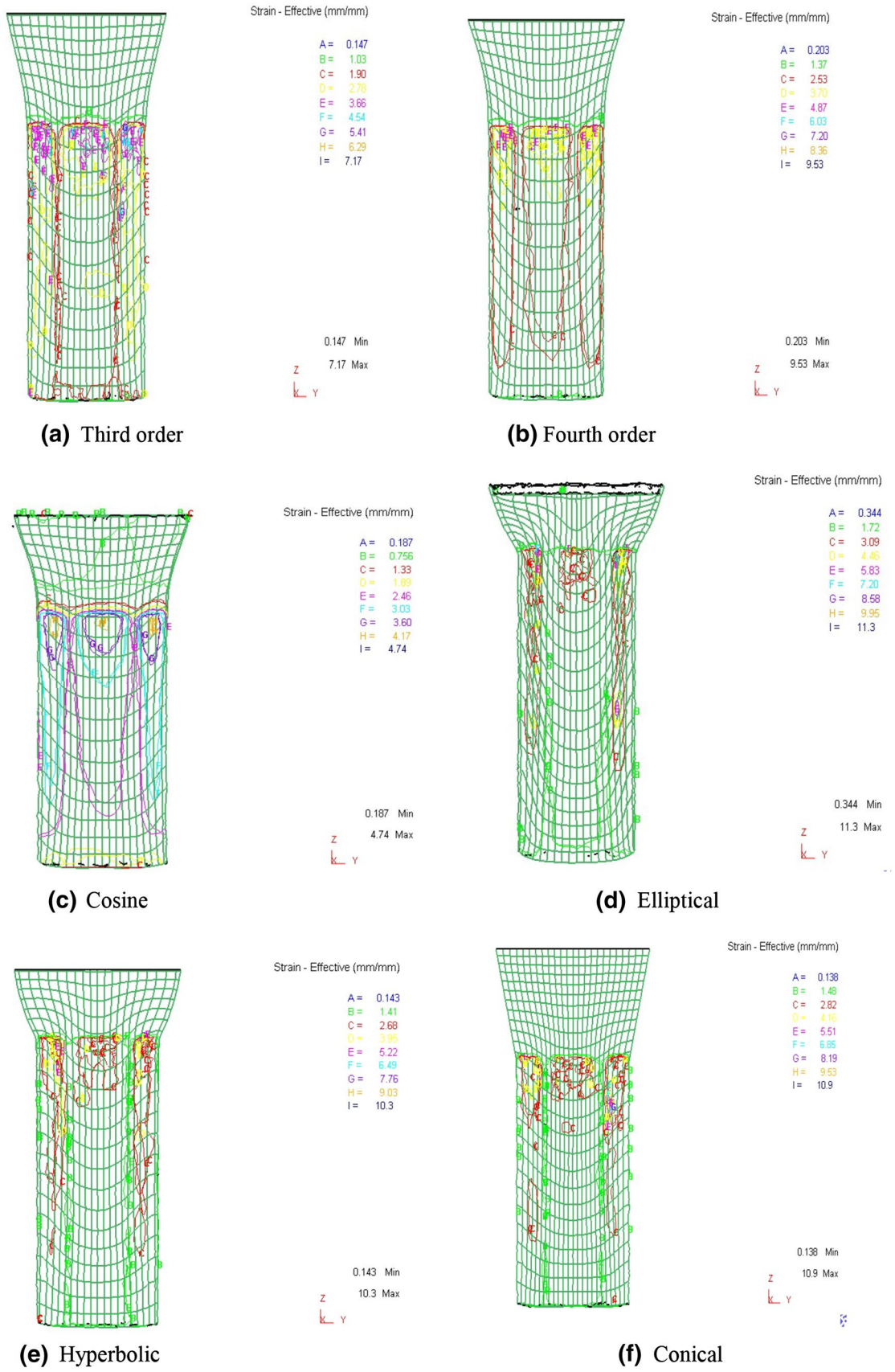

Fig. 19 Strain distribution for six different profiles

Fig. 20 Specially machined extrusion die with cosine profile

Fig. 21 Extruded hexagonal section

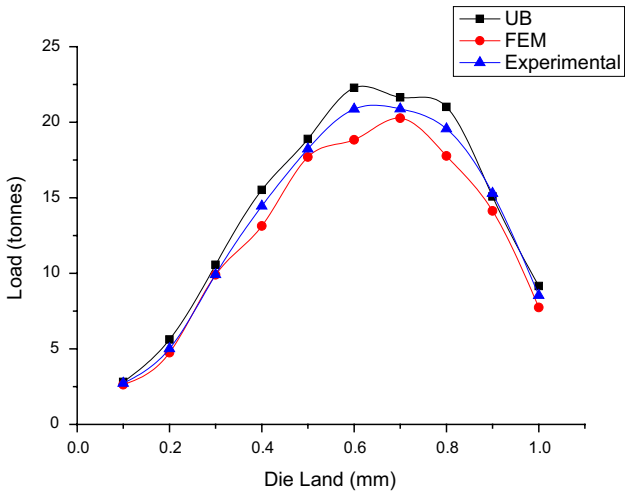

Fig. 22 Extrusion load curve (comparative)

Figure 22 shows the graphical representation of load requirement versus die land for the results incurred through the upper bound technique, FEM simulation and the experiment. Higher load consumption in experimental study than the FEM simulation reveals the lubrication complication prevailing over the die surface. Experimental results have not incurred any significant deviations from the analytical method and FEM simulation.

8 Conclusion

After an exhaustive study of SiC reinforced Al composite through UB, FEM and experiment method for six various die profiles, the following conclusions have been arrived.

1. By means of a suitable design of the die geometric shape, it is possible to obtain a favourable positioning or a dead zone size reduction. This determines the importance of reduction of friction in the deformation zone and of the extrusion load as well.
2. It is concluded that during the extrusion of SiC DRMM composite, the reinforced SiC particles moves in two ways. They flow either with the matrix material or move with an abrading action over the die surface.
3. The SiC particles found in the outermost layer of the composite material may adhere to the die entrance and scratch the die bearing surfaces thereby inducing a higher frictional effect.
4. Development of dead zone found to be in two sections as primary and secondary dead zone. Higher development of dead zone accompanying with greater frictional force causes the outer most layer of the billet into more severe deformation than the central part.
5. Higher dead metal zone, adhering and agglomeration of SiC particles, development of scratches are concluded as the potential constraints, when the SiC particle reinforced billet is forced into extrudate.
6. Uniform curvature effect right from starting to end of the cosine curve profile facilitates the homogeneous flow of MMC material with negligible effect of adhering and agglomeration of SiC particles and also minimizes the effect of scratching the die entrance and bearing surface with nullifying effect of dead metal zone.
7. Benefit of cosine die profile over the rest of five different profiles is learnt from the metal flow analysis through upper bound technique, Finite element technique and the experimental study.
8. It is realised that the cosine profile die is the most optimised die profile for the extrusion of SiC DRMM Al 6061 composite with aforementioned volume fraction and particle size, because the results obtained for the six various profiles from upper bound technique, Finite element technique and experimental method have not incurred any significant deviations to each other.

Acknowledgments This study was supported by Advance Forming Technology Corporation.

References

1. Narayanasamy R, Ponnalugusamy R, Venkatesan R, Srinivasan P (2006) An upper bound solution to extrusion of circular billet to circular shape through cosine dies. Int J Mater Des 27:411–415
2. Narayanasamy R, Ponnalugusamy R, Srinivasan P (2005) Design and development of stream lined extrusion dies a Bezier curve approach. Int J Mater Process Technol 161:375–380
3. Venkatareddy N, Dixit PM, Lal GK (1995) Die design for axisymmetric extrusion. International. J Mater Process Technol 55:331–339
4. Seo YH, Kang CG (1999) Effects of hot extrusion through a curved die on the on the mechanical properties of SiC/Al composites fabricated by melt- stirring. J Compos Sci Technol 1999:643–654
5. Herba EM, McQueen HJ (2004) Influence of particulate reinforcements on 6061 materials in extrusion modeling. J Mater Sci Eng A 372:1–14
6. Nair F, Baki Karamis M (2010) An investigation of the tribological interaction between die damage and billet deformation during MMC extrusion. Tribol Int 43:347–355
7. Gordan WA, Van CJ, Moon YH (2012) Minimizing distortion during extrusion using adaptable dies. Int J Mech Sci 62:1–7
8. Gouveia BPPA, Rodrigues JMC, Bay N, Martins PAF (2000) Deformation analysis of the round to square extrusion : a numerical and experimental investigation. J Finite Elem Anal Des 35:269–282
9. Venkatesh C, Venkatesan R (2014) Design and analysis of stream lined extrusion die for round to hexagon through Area mapping technique, Upper bound technique and Finite element method. J Mech Sci Technol. Accepted and may appear in May-2014 issue
10. Avitzur B (1968) Metal forming : processes and analysis. McGraw Hill, New York
11. Fischer-Cripps AC (2011) Nanoindentation. Springer, New York
12. DEFORM-3D V6.1-Manual